ACS APPLIED MATERIALS & INTERFACES

Research Article

www.acsami.org

Three Dimensional Ag_2O/TiO_2 Type-II (p−n) Nanoheterojunctions for Superior Photocatalytic Activity

Debabrata Sarkar,[†] Chandan. K. Ghosh,[†] S. Mukherjee,[†] and Kalyan K. Chattopadhyay*[,†,‡]

[†]School of Material Science and Nanotechnology, Jadavpur University, Kolkata 700 032, India

[‡]Thin Film and Nanoscience Laboratory, Department of Physics, Jadavpur University, Kolkata 700 032, India

Supporting Information

ABSTRACT: Type-II p−n junction three-dimensional Ag_2O/TiO_2 microspheres have been fabricated by assembling p-type Ag_2O nanoparticle on n-type TiO_2 3D microsphere. Ag_2O/TiO_2 microsphere nanoheterojunctions were obtained by hydrothermal synthesis of TiO_2 microspheres at 180 °C followed by photoreduction of $AgNO_3$. The samples were carefully characterized by X-ray diffraction (XRD), transmission electron microscopy (TEM), field-emission scanning electron microscopy (FESEM), and energy dispersive X-ray analysis (EDX). The photocatalytic activity toward degradation of methyl orange (MO) aqueous solution under UV light was investigated. The result showed that type-II p−n nanoheterojunctions Ag_2O/TiO_2 significantly enhanced the photocatalytic degradation compared to n-type TiO_2 microsphere. It was found that the photocatalytic degradation followed the pseudo first-order reaction model. In particular, heterostructure with molar ratio of TiO_2 and $AgNO_3$ of 4:1 exhibited best photocatalytic activity and the corresponding apparent first-order rate constant of 0.138 min^{-1} which is 4 times than that of pure n-type microsphere.

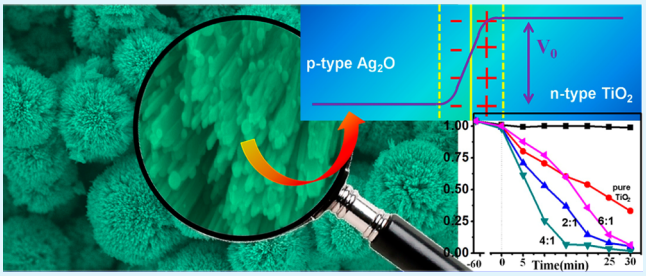

KEYWORDS: *nanoheterojunctions, 3D p-type Ag_2O/n-type TiO_2, UV photocatalysis*

1. INTRODUCTION

Since the discovery of the phenomenon of photocatalytic splitting of water under ultraviolet light by Fujishima and Honda in 1972,[1] titanium dioxide (TiO_2) has been proven to be the most suitable and promising semiconductor catalyst in heterogeneous photocatalysis for its high physical and chemical stability, nontoxicity, effectivity, high oxidizing power, and low price.[2,3] Photocatalysis occurs when the semiconductor catalyst is exposed to a photon of energy equal to or higher than the band gap of the semiconductor. Absorption of photon by semiconductor creates electrons (e^-) in the conduction band and holes (h^+) in valence band. The photogenerated e^-/h^+ pair reacts with the adsorbed molecules such as adsorbed oxygen, surface hydroxyls groups, or water, ultimately producing the high oxidizing species radicals which can oxidize organic molecules present in the solution into carbon dioxide and water.[4] The electron−hole recombination and low interfacial charge transfer rates are responsible for the low quantum yields. For further improvement of photocatalytic activity of TiO_2, numerous efforts have been made, including cation- or anion-doping, formation of heterostructures, and so on.[5−11] Researchers found that TiO_2 based heterojunction, such as deposited noble metals (Ag, Au, Pt, or Pd) on the TiO_2 surface and semiconductor (CdS, SnS_x, V_2O_5, Ag_2O, WO_x, Bi_2O_3, $ZnMn_2O_4$, $FeTiO_3$, $LaVO_4$) couple with TiO_2, could effectively improve photocatalytic efficiency.[2,12−19] For this purpose, silver and silver based oxide are the most suitable for industrial application because of its high efficiency, low cost, and easy preparation. A literature survey indicated that studies on the TiO_2/Ag_2O system are extremely scanty; particularly, there is no report on the three-dimensional heterostructures of such system. Ag_2O is a p-type semiconductor with an energy band gap of 1.46 eV.[20] All these properties of Ag_2O are beneficial for the formation of p−n nanoheterojunction with TiO_2 for superior photocatalyst. The photogenerated electrons can move to the conduction band of n-type TiO_2 and photogenerated holes can move to the valence band of p-type Ag_2O which promote an interfacial electron transfer process and reduce the charge recombination on the semiconductor.

On the other hand, the photocatalytic activity is related with the size, shape, surface area, morphology, and the dimensionality of the catalysts.[21] Nanometer-scaled TiO_2 based catalyst, such as nanoparticles, nanorods, nanosheets, and nanotubes exhibit promising performance as a photocatalyst., but they tend to aggregate during the photocatalysis process, which reduces the active surface area.[22] Many studies found that three-dimensional (3D) hierarchical nanoarchitectures assembly of one dimension (1D) nanorods, nanowires, nanotubes, etc. are highly desired due to their high surface-to-volume ratio, high organic pollutant adsorption, and excellent incident light scattering within the structures.[23] Recently, Zhou et.al reported 3D rutile TiO_2 with different nanostructures in detail.[24] In

Received: October 5, 2012
Accepted: December 17, 2012
Published: December 17, 2012

addition, after photocatalysis reaction, the 3D Ag_2O/TiO_2 heterojunction nanostructures can be completely separated and recovered from the treated aqueous solution. To the best of our knowledge, this is the first time that 3D p-type Ag_2O/n-type TiO_2 heterostructure has been fabricated and photocatalysis performances have been explored.

In the present paper, we have successfully synthesized uniform 3D TiO_2 hierarchically microspheres in high yields (100% morphological yield) by a modified hydrothermal method and 3D Ag_2O/TiO_2 p−n nanoheterojuncions were fabricated in different molar ratio of TiO_2 and $AgNO_3$ using a UV lamp by the photochemical reduction technique. Scheme 1

Scheme 1. Schematic of Fabrication Route to p-Ag_2O/n-TiO_2 Nanoheterjunction

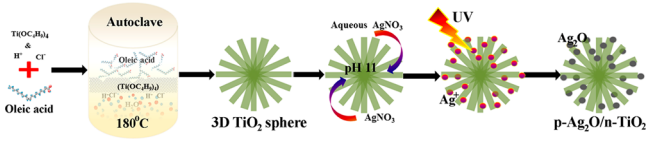

illustrates the formation procedure of 3D p-Ag_2O/n-TiO_2 nanoheterojunction. The prepared samples were characterized by X-ray diffraction (XRD), field-emission scanning electron microscopy (FESEM), high resolution transmission electron microscopy (HRTEM), X-ray photoelectron spectroscopy (XPS), and UV−vis spectroscopy. The photocatalytic activity of these hybrid heterostructures was carefully investigated by degradation of methyl orange (MO) dye under UV irradiation. The 3D Ag_2O/TiO_2 p−n junction heterostructure accelerated the surface electron transfer rate, and the inner electric field in the interface of p−n heterojunction acted as a potential barrier to prevent the recombination of the electron−hole pair.

2. EXPERIMENTAL SECTION

Titanium butoxide ($Ti(OC_4H_9)_4$) was purchased from Sigma Aldrich. Oleic acid, hydrochloric acid (HCl, about 35% by weight), and silver nitrate ($AgNO_3$) were supplied by Merck India.

2.1. Preparation of Photocatalysts. *2.1.1. 3D TiO_2 Microspheres.* 3D dandelion-like TiO_2 microspheres were prepared by a hydrothermal method, and the details of the synthetic procedure were described in our previous paper.[25] Briefly, at first, 4 mL of titanium butoxide was mixed with 2 mL of 35% HCl. Then, the mixture of titanium butoxide and HCl was added slowly into 20 mL of oleic acid under magnetic stirring. After the mixture was stirred for 15 min, the total[26] solution was transferred into a Teflon lined autoclave of 50 mL capacity and the hydrothermal synthesis was conducted in an electric oven at 180 °C for 4 h. After naturally cooling down, the products were collected, washed several times with absolute ethanol, and then dried in air at 70 °C for 12 h. The obtained 3D dandelion-like TiO_2 powders were ready for further characterization.

2.1.2. Ag_2O Deposition onto the 3D Dandelion-Like TiO_2 Microspheres. All the deposited samples were synthesized via a photoreduction process. Initially, 0.4 g of the as-prepared 3D microspheres was dispersed into 50 mL of distilled water. NH_4OH was dropwise added to adjust the pH of suspension to about 11. Then, an appropriate amount of $AgNO_3$ was added into the solution. The molar ratio of TiO_2 to $AgNO_3$ was controlled to be 2:1, 4:1, and 6:1. After the mixture was stirred for 2 h, the solution was irradiated for 1 h by a 40 W Ultraviolet lamp under magnetic stirring. After illumination, the obtained dark brown Ag_2O/TiO_2 was thoroughly washed with distilled water and dried at room temperature. For comparing photocatalytic activity of 3D Ag_2O/TiO_2 microspheres with Ag_2O/TiO_2 nanoparticles, we further extended this method to synthesize Ag_2O/TiO_2 nanoparticles using commercially available Degussa P25 (TiO_2) powder (average particle size 21 nm) under the identical experimental conditions.

2.1.3. Sample Characterization. The morphology of the sample was examined with a field emission scanning electron microscope (FESEM, S-4800, Hitachi) equipped with an energy dispersive X-ray (EDX), high-resolution transmission electron microscope (HRTEM, JEOL 2010). The crystallinity and phase of Ag_2O/TiO_2 microspheres was determined by X-ray diffraction (XRD, D8 Advanced, Bruker). The elemental compositions and chemical status were analyzed by X-ray photoelectrons spectroscopy (XPS, HSA-3500, SPECS, Germany). The carbon C 1s line with position at 284.5 eV was used as a reference to correct the charging effect.

2.1.4. Photocatalytic Experiments. Photocatalytic activity of the synthesized pure n-type TiO_2 and p-Ag_2O/n-TiO_2 microspheres was evaluated with MO dye as the probe molecules under UV irradiation. Forty milligrams of the sample was dispersed within a 40 mL dye solution with a concentration of 10^{-5} M in a 100 mL quartz beaker. Before the photocatalytic activity test, the suspension was continuously stirred in the dark without irradiation for 1 h to establish the adsorption/desorption equilibrium of the dye on the nanorod surface of the microsphere. One 40 W UV tube (Phillips) with a maximum emission at 254.6 nm was used as the UV resource, and the UV source to suspension surface distance was kept at 15 cm. At a given time interval, 3 mL of suspension was withdrawn and analyzed after removal of catalyst particles by centrifugation at 12 000 rpm for 60 min. The absorbance spectra of the centrifuged solutions were recorded using a UV−vis spectrometer (Shimadzu 2550). As a comparison, the photocatalytic activities of Ag_2O/TiO_2 nanoparticles were also measured using the same parameters.

3. RESULTS AND DISCUSSION

3.1. Phase and Morphology of n-Ag_2O/p-TiO_2 Photocatalysts. Crystallinity of the 3D Ag_2O/TiO_2 microsphere nanoheterojunction with different molar ratio of TiO_2 and $AgNO_3$ is analyzed using XRD as shown in Figure 1a. It can be found that the characteristic peaks for both pure-TiO_2 and Ag_2O/TiO_2 corresponding to rutile phase are detected (JCPDS

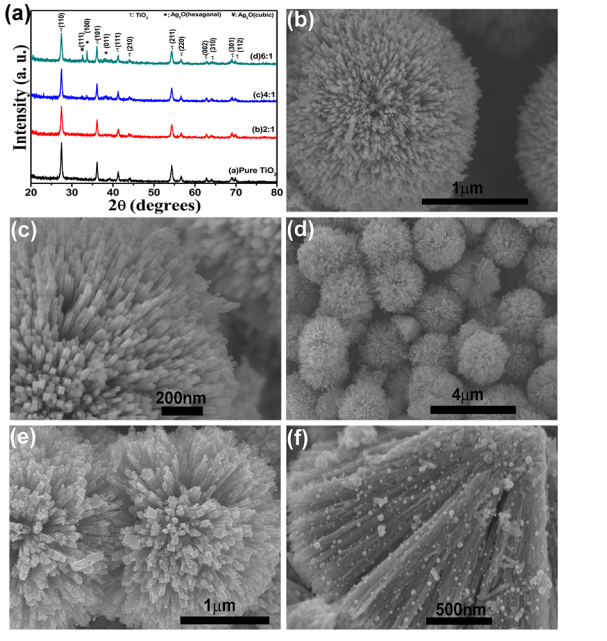

Figure 1. (a) XRD patterns of pure TiO_2 and Ag_2O/TiO_2 heterostructure with different molar ratio of TiO_2 and $AgNO_3$. (b, c) Typical FESEM images of the pure TiO_2 microspheres. (d−f) FESEM images of Ag_2O/TiO_2 heterostructure with different molar ratio of TiO_2 to $AgNO_3$: (d) 2:1, (e) 4:1, and (f) 6:1.

dx.doi.org/10.1021/am302136y | ACS Appl. Mater. Interfaces 2013, 5, 331−337

No.78-2485). XRD patterns for 4:1 and 6:1 exhibit peaks corresponding to hexagonal Ag_2O {100} and {011} planes at 33.6° and 38.39°, respectively (JCPDS No.72-2108). An additional peak for cubic Ag_2O was also detected at 32.56° (JCPDS No.76-1393). For 2:1, Ag_2O peaks could not be seen probably because of low content of $AgNO_3$. It has been found that Ag_2O/TiO_2 was obtained by UV reduction of $AgNO_3$ under 1 h UV irradiation. Actually, reduction of $AgNO_3$ to Ag_2O or further reduction to Ag^0 is dependent on the exposure time. Hence, for higher UV exposure time, Ag_2O is decomposed into Ag atoms and AgO but the AgO phase is unstable at room temperature compared with Ag_2O. AgO readily undergoes photoreduction to form metallic Ag and O_2. The photodecomposition of Ag_2O to metallic silver can be described as follows:

$$Ag_2O \rightarrow AgO + Ag$$

$$AgO \rightarrow Ag + \frac{1}{2}O_2$$

The XRD pattern of the samples with different UV irradiation time is shown in Figure S1, Supporting Information. It clearly shows the presence of metallic Ag at 2θ = 38.11° {111} (JCPDS No.04-0783). No peaks of other silver oxides were observed. Therefore,during photoreduction, the Ag^+ to Ag_2O or Ag^0 can be mediated by the time of irradiation with UV light.

The morphology and microstructural details of the prepared TiO_2 microsphere and Ag_2O/TiO_2 p−n heterostructure were investigated by FESEM and HRTEM observation as shown in Figures 1 and 2. Figure 1b shows pure TiO_2 microsphere with

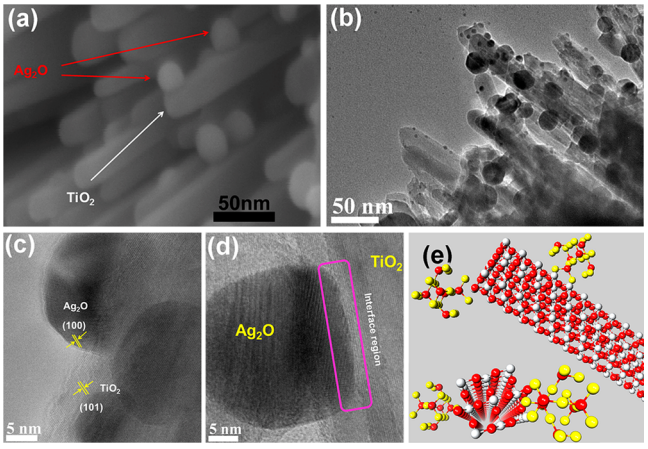

Figure 2. (a) High magnification FESEM image of heterojunction; (b−d) TEM and HRTEM images of the TiO_2/Ag_2O heterojunction. (e) Schematic atomic model.

an average diameter of about 2 μm. High magnification images of the same samples, which are shown in Figure 1c, illustrate that each microsphere consists of nanorods with square-shaped ends of diameter about 20 nm. The illustrative FESEM images of Ag_2O/TiO_2 nanoheterostructure with different molar ratio of TiO_2 to $AgNO_3$ are shown in Figure 1d−f which displays the Ag_2O nanoparticles are uniformly covering the surface of microspheres. Figure 1d shows that the catalyst consists of large quantities of spherical architectures. The cross section image (Figure 1f) shows the nanorods radiate from a center and Ag_2O nanoparticle attached throughout the surface of the nanorods.

Figure 2a,b shows that Ag_2O nanoparticles of size 5−20 nm are tightly coupled on the TiO_2 nanorod surface within the microspheres. Typical transmission electron microscopy (TEM) images were used to further confirm the formation of heterostructure. Figure 2b shows the respective TEM images of the TiO_2/Ag_2O nanostructure. Meanwhile, the high-resolution TEM images of the region marked by a red square are displayed in Figure 2c,d, which revealed simultaneous presence of the crystalline TiO_2 and Ag_2O. The interplanar spacing of 0.266 nm corresponds to the (100) plane of Ag_2O, while 0.249 nm corresponds to the (101) plane of rutile TiO_2. A continuity of lattice fringes between the interface of TiO_2 and Ag_2O is shown in Figure 2d which indicates the formation of p−n nano-heterojunction. On the basis of the above FESEM and HRTEM analysis, an atomic model of this heterostructure is illustrated in Figure 2e where red and white balls correspond to O and Ti atoms and yellow balls correspond to Ag atoms.

Figure 3b is the corresponding energy dispersive X-ray spectroscopy of the sample shown in Figure 3a, which shows

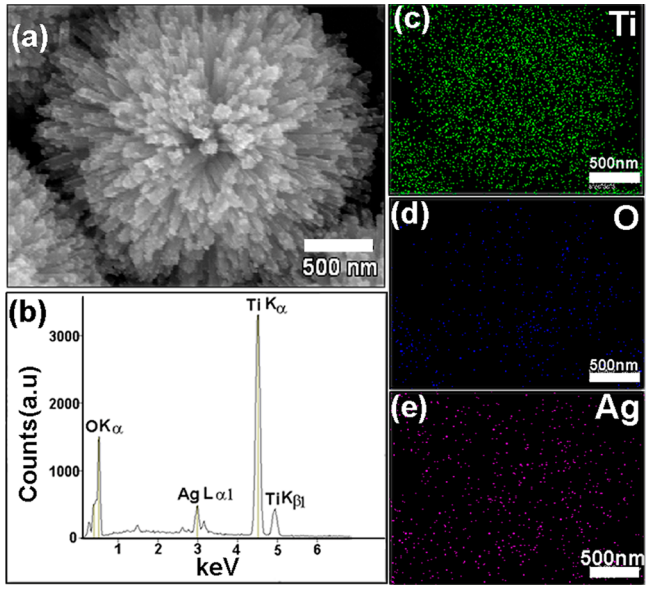

Figure 3. EDX and elemental mapping of 3D Ag_2O/TiO_2 microsphere.

that the obtained microspheres are composed of the elements Ti, O, and Ag. Figure 3c−e corresponds to the EDX elemental mapping images of Ti, O, and Ag which shows the distribution of the Ag ions on the surface is homogeneous.

The elemental compositions and chemical status of the Ag_2O/TiO_2 nanoheterostructure were analyzed by XPS. Figure S2, Supporting Information, shows the full-range XPS spectrum of the Ag_2O/TiO_2 nanoheterojunction, revealing only Ti, O, Ag, and a carbon peak (C 1s). Figure 4 demonstrates the high-resolution XPS spectra for Ag $3d_{3/2}$ and Ag $3d_{5/2}$ photoelectrons at 373.7 and 367.7 eV, respectively. These binding energies are consistent with values reported for Ag_2O.[26−29] This indicates that the silver exists in one valence state (Ag^+) in the heterojunction confirming synthesis of Ag_2O, which supports XRD results.

The actual Ag_2O content within each sample were measured from XPS spectra considering atomic sensitivity factors of different elements.[30,31] These are found to be 0.22, 0.3, and 0.59 wt % for 6:1, 4:1, and 2:1 3D Ag_2O/TiO_2 microspheres

dx.doi.org/10.1021/am302136y | ACS Appl. Mater. Interfaces 2013, 5, 331−337

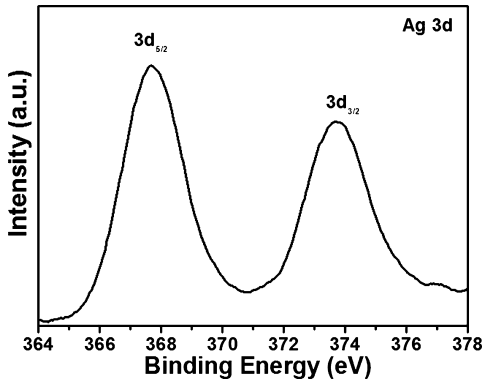

Figure 4. High-resolution XPS spectra for the Ag $3d_{5/2}$ and Ag $3d_{3/2}$.

whereas initially calculated loading percentages were 0.24, 0.36, and 0.72 wt % for these three samples, respectively. These results clearly confirm that the whole $AgNO_3$ does not transform into Ag_2O. The detailed calculated loading percentages are shown in the Supporting Information.

3.2. Photocatalytic Activities. Photocatalytic performances of pure-TiO_2 and Ag_2O/TiO_2 heterostructure, obtained in different molar ratio of TiO_2 and $AgNO_3$, were comparatively evaluated by measuring the degradation of MO aqueous solution under UV irradiation. The change in MO concentration as a function of UV irradiation time is represented in Figure 5a which shows that without catalyst the concentration of MO does not change for every measurement. From Figure S3, Supporting Information, it can be seen that the absorption spectra of MO at 463 nm decreased rapidly under UV irradiation. The MO decolorization rate for pure n-type TiO_2 microspheres after 30 min UV light irradiation can only approach 67%. It was found that, for Ag_2O/TiO_2 p−n nanoheterojunction, the degradation increases significantly with increasing the molar ratio of TiO_2 and $AgNO_3$ and reaches a maximum at 4:1 ($TiO_2/AgNO_3$ = 4:1). With further increase of molar ratio, photocatalytic degradation decreases. Therefore, the optimum molar ratio of TiO_2 and $AgNO_3$ is 4:1 which degrades the MO within 15 min of UV irradiation which is 3 times faster than that of the pure TiO_2. The degradation or decolorization percentages of the catalysts after 15 and 30 min irradiation are shown in Figure 5c. The observed photocatalytic performance is far better than compared to most of the reported nanostructures which has been summarized in Table 1. The photocatalytic degradation kinetic was investigated; the linear simulation of degradation of dye concentration can be accounted for by a pseudo first-order model, called the Langmuir−Hinshelwood (L-H) model. The L-H model is well established for heterogeneous photocatalysis (at low dye concentration).[42] The relevant equation is as below:

$$r = -\frac{dC}{dt} = k_{app}C$$

where r was the degradation rate, C_t/C_0 is the ratio of the concentration dye after various intervals of time and concentration of the dyes at adsorption−desorption equilibrium, and k_{app} was the apparent first-order rate constant (min^{-1}). We are able to find out k_{app} from the gradient of the graph of $\ln(C_0/C_t)$ versus time (t) which is shown in Figure 5b. The k_{app} value for the pure TiO_2 microsphere is estimated to be 0.034 min^{-1}, and those estimated for Ag_2O/TiO_2 heterostructure lie within the range of 0.033−0.138 min^{-1}. The value of k_{app} for 4:1 Ag_2O/TiO_2 sample is 0.138 min^{-1} which is 4 times larger than that of others. The dye color change sequence during degradation can also be visualized from the digital photograph (Figure 5d) which shows the intense orange color

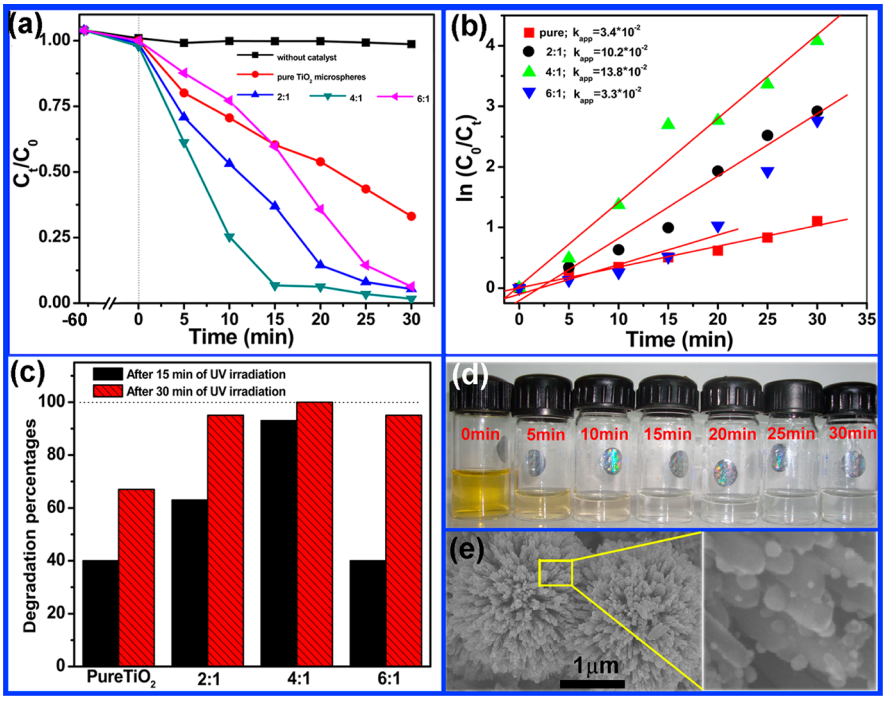

Figure 5. (a) Photocatalysis degradation profiles of MO under UV irradiation. (b) Kinetic plot with different molar ratio of TiO_2 to $AgNO_3$. (c) Degradation percentages after 15 and 30 min irradiation. (d) Digital photograph of the decolorization of MO after different UV exposure times for $TiO_2/AgNO_3$ = 4:1. (e) 3D heterostructure after photocatalytic performance.

Table 1. Performances of Photocatalytic Activity in the Reported Literature

catalyst used and amount	conc. and volume of MO	UV light source	degradation time (min)	degradation %	reference
3D Ag_2O/TiO_2 nanoheterojunction (40 mg)	10^{-5} M, 40 mL	40 W	15, 30	93, 100	our work
Pt nanocrystals/titante nanobelts (50 mg)	10^{-4} M L^{-1}, 50 mL	125 W	300	100	32
Au/Pt/ZnO hollow nanoparticles (10 mg)	10^{-5} M, 20 mL	125 W, λ = 365 nm	40	90	33
porous ZnO nanotubes (15 mg)	10^{-5} M, 80 mL	125 W	60	100	34
TiO_2/graphene sheets (GS)			50	87	35
Ag_2O/TiO_2 nanobelts (20 mg)	20 mg/L	20 W	15	85	4
ZnO nanoplate−nanowire architecture	6×10^{-5} M, 20 mL	300 W	55	100	36
SnO_2/ZnO heterojunction (30 mg)	10^{-5} M, 90 mL	2 × 4 W	35−40	100	37
nanocrystalline $Sr_{0.25}H_{1.5}Ta_2O_6{\cdot}H_2O$ (80 mg)	20 mg L^{-1}, 160 mL	3 × 4 W	80	77	38
gold nanoparticle/ZnO (10 mg)	20 mg L^{-1}		60	95	39
1D TiO_2−graphene nanocomposite (10 mg)	100 mg L^{-1}, 50 mL	125 W	180	82	40
rod-like TiO_2 (A) (45 mg)	4×10^{-5}M, 45 mL	100 W	80	100	41
3D porous ZnO nanostrip (30 mg)	5×10^{-5}M, 50 mL	300 W	60	100	22

of the MO dye gradually decreases with increasing UV irradiation time and irradiation dye color almost changes from orange to clear. Figure 5e shows that after photocatalytic performances the three-dimensional structure as well as nanoparticle attachment remains the same which is necessary for practical application point of view. Figure S4, Supporting Information, shows the XRD patterns for photocatalyst after photocatalytic performance which confirms the phase of Ag_2O on the TiO_2 nanorod surface.

For comparison, the photocatalytic behavior of Ag_2O/Degussa P25 was also measured. P25 (Degussa) is known as one of the best commercially available TiO_2 nanoparticles with average particle size of 21 nm. The morphology of the prepared Ag_2O/P25 nanoparticles is shown in Figure S5, Supporting Information. The photocatalytic activities of p-Ag_2O/n-TiO_2 microspheres and Ag_2O/P25 nanoparticles for samples 2:1 and 4:1 (molar ratio of $AgNO_3$ to TiO_2), measured under identical conditions, are presented in Figure 6, from which it is clear that

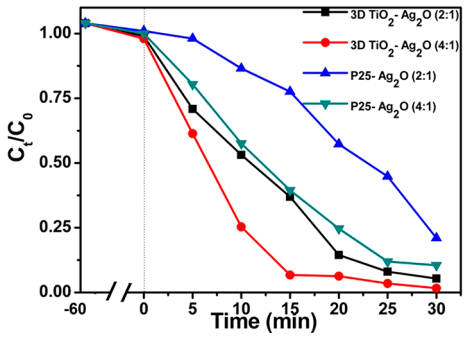

Figure 6. Photocatalysis degradation profiles of MO for p-Ag_2O/n-TiO_2 microspheres and Ag_2O/P25 nanoparticles with molar ratios of TiO_2 to $AgNO_3$ of 2:1 and 4:1.

the almost complete degradation of MO dye was observed after 15 min of UV irradiation for 3D p-Ag_2O/n-TiO_2 microspheres, while after 15 min for Ag_2O/P25 nanoparticles (sample 4:1), the degradation is only about 60%. Therefore, the as-synthesized 3D p-Ag_2O/n-TiO_2 microspheres exhibited higher photocatalytic activity than the P25/Ag_2O nanoparticle. Although P25/Ag_2O nanoparticle shows a definite photocatalytic activity, it was difficult to separate it from the photocatalytic medium after application. Whereas after the photocatalysis reaction, the 3D Ag_2O/TiO_2 heterojunction nanostructures are completely separable and can be recovered from the treated aqueous solution.

The stability is very important for recycling of catalysts based on its importance for practical application. In this work, to investigate the photocatalytic stability of Ag_2O/TiO_2 3D microspheres in the recycled process, five cycles of photodegradation of MO were conducted taking 2:1 and 4:1 Ag_2O/TiO_2 catalyst as a typical sample. The recovered Ag_2O/TiO_2 nanostructures were reused in the next cycle. Figure 7 shows

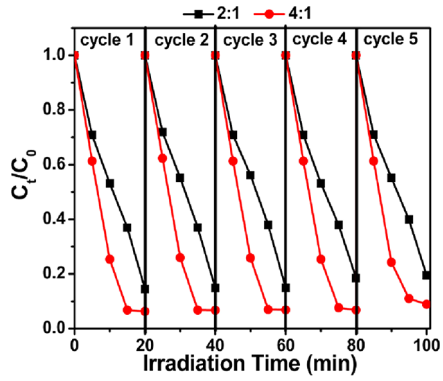

Figure 7. Recycled performances in the presence of p-Ag_2O/n-TiO_2 heterojunction for photodegradation of MO dye.

that there is no obvious reduction of the photocatalytic degradation efficiency after five repeated cycles. These results indicate the good stability and reusability of our 3D Ag_2O/TiO_2 p−n nanoheterojunction.

As degradation occurs at the catalyst surface, surface area is an important parameter for photocatalytic activity. The specific surface area, S_A, was calculated from Brunauer−Emmett−Teller (BET) model[43]

$$S_A = \frac{6}{\rho d}$$

where d is the particle size and ρ is the density of the TiO_2. The estimated particle size was calculated using the Debye−Scherrer formula (Supporting Information). The specific surface area of the bare TiO_2 microsphere and 6:1, 4:1, and 2:1 (Ag_2O/TiO_2 microsphere) was calculated to be 54.6, 57.9, 58.1, and 61.7 m^2/g, respectively. The above results obviously show that effective surface area of the Ag_2O nanoparticles accumulated on TiO_2 surface was larger than the surface of bare TiO_2 microsphere. Thus, the larger specific surface area of 3D p-

dx.doi.org/10.1021/am302136y | ACS Appl. Mater. Interfaces 2013, 5, 331−337

Ag_2O/n-TiO_2 microspheres will increase the photocatalytic reaction sites for the adsorption of reactant molecules and promote the efficiency of the electron−hole separation. It was found that, for Ag_2O/TiO_2 p−n nanoheterojunction, the degradation increases significantly with increasing the specific surface area and reaches a maximum at 4:1 ($TiO_2/AgNO_3$ = 4:1). Therefore, the specific surface area is not the sole parameter in determining the photocatalytic activity.

3.3. Mechanism on Enhancement of Photocatalytic Activity. The enhanced photocatalytic performance of the heterostructure can be explained by assuming the formation of p−n junction, and a possible proposed energy band structure of Ag_2O/TiO_2 p−n junction is elucidated schematically in Figure 8. Ag_2O is a p-type narrow band gap semiconductor with

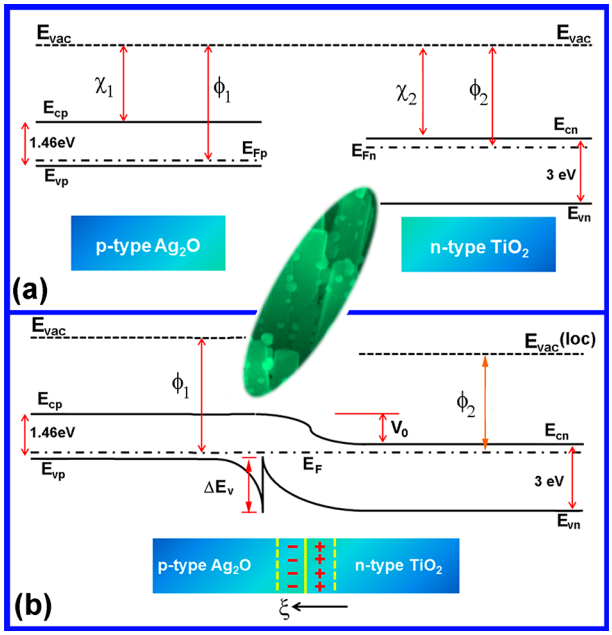

Figure 8. (a) The energy band structures of Ag_2O and TiO_2 before formation of heterojunction and (b) the energy band structures of p-Ag_2O/n-TiO_2 heterojunction at equilibrium (E_{vac}: vacuum level; E_F: Fermi level; ϕ: work function; χ: electron affinity).

ionization potential of 5.3 eV[44] and work function of 5.0 eV,[45] while rutile TiO_2 is a n-type wide band gap (3 eV) semiconductor with electron affinity of 4.0 eV[46] and work function of 4.5 eV.[47] On the basis of the above values, the energy band structure of the Ag_2O and TiO_2 before contact is shown in Figure 8a. When Ag_2O nanoparticles are attached onto the TiO_2 nanorod surface, type-II p−n nanoheterojunctions are formed at the interface and electron transfer occurred from TiO_2 to Ag_2O until their Fermi levels align; i.e., the semiconductor system reaches the thermal equilibrium state. Therefore, due to alignment of Fermi level, band bending would be expected which is schematically shown in Figure 8b. Because of carrier concentration gradients, electrons diffuse from n-type to p-type region and holes diffuse from the p-type to n-type region. At the junction in equilibrium, the n-type TiO_2 regions have a positive charge, while p-type Ag_2O has a negative charge, so that an opposing electric field (ξ) is created at the junction and there is an equilibrium potential difference V_0 across the transition region, called contact potential. During the photocatalysis process, the photogenerated electrons can move to the conduction band (E_{cn}) of the n-type TiO_2 and holes can move to the valence band (E_{vp}) of the p-type Ag_2O due to the built in electric field at the p-Ag_2O/n-TiO_2 nanojunction and retard the recombination. The photocatalytic activity was found to be increased with increasing molar ratio of TiO_2 and $AgNO_3$. Furthermore, with increasing molar ratio of $TiO_2/AgNO_3$, the number of nanoheterojunctions increases and a larger number of electron−hole pairs within the space charge region are efficiently separated by the electric field. The optimum content of Ag_2O could be related to the light penetration depth in the space charge layer and also the amount of exposed surface area of TiO_2. Recently, Hui et al. also reported existence of an optimal percentage of AgBr in AgBr/$BiPO_4$ p−n junction for the best photocatalytic performance.[48]

On the basis of the above experimental results and discussion, a possible mechanism for dye degradation under UV irradiation is proposed in Scheme 2. When Ag_2O/TiO_2 p−n heterostructure is radiated by UV light with photon energy equal or higher to the band gaps of Ag_2O and TiO_2, both Ag_2O and TiO_2 could be simultaneously excited to form electron−hole pairs. As per Figure 6b, due to band banding and under the influence of the electrostatic field ξ in the junction, the photogenerated electrons easily transfer from the CB of Ag_2O to that of TiO_2 and holes transfer from the VB of TiO_2 to that of Ag_2O. The photogenerated electrons react with adsorbed O_2 and H_2O on the surface of the heterostructure and produce superoxide radical anions such as $\cdot O_2^-$, OOH, and OH^-. The photogenerated holes can be trapped by H_2O and OH^- to further produce ·OH and OH^- species. During the photocatalytic reaction process, it is observed that the photogenerated electron and hole pairs were separated efficiently on the p-type Ag_2O/n-type TiO_2 heterojunction interface and then participated in a chemical reaction and produced powerful superoxide radical as well as oxidizing agent ($\cdot O_2^-$, ·OH, ·OOH, and OH^-) that decomposed the organic dyes.

Scheme 2. Proposed Photocatalytic Mechanism of p-Ag_2O/n-TiO_2 Nanoheterjunction

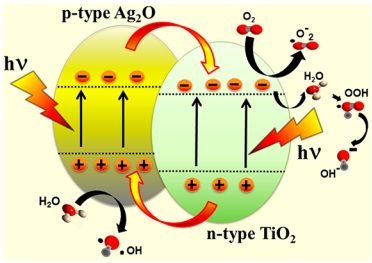

4. CONCLUSIONS

Three dimensional Ag_2O/TiO_2 p−n nanoheterojunction has been successfully prepared via a low-temperature hydrothermal and UV photochemical reduction process. Uniform assembly of Ag_2O nanoparticle was observed on the surface of the TiO_2 which produces a large number of p−n nanoheterojunctions. The Ag_2O/TiO_2 nanoheterostructure promotes the charge separation due to built in electrostatic field at the junction and exhibits higher photocatalytic activity than that of pure TiO_2. Due to their large surface area, high surface to volume ratios, superior photocatalytic activity, and unique stable three-dimensional structures, optimum molar ratios of TiO_2 and

dx.doi.org/10.1021/am302136y | ACS Appl. Mater. Interfaces 2013, 5, 331−337

$AgNO_3$ will greatly promote their industrial application to eliminate the organic pollutants from wastewater.

■ ASSOCIATED CONTENT

Supporting Information

XRD pattern with UV irradiation time 3 h and 5 h, full-range XPS spectrum of Ag_2O/TiO_2 nanoheterojunctions, changes in absorption spectra of MO in the presence of Ag_2O/TiO_2 catalyst, XRD patterns for Ag_2O/TiO_2 nanoheterojunctions before and after photocatalytic performance, and FESEM images of Ag_2O/P25 nanoparticles. This information is available free of charge via the Internet at http://pubs.acs.org/.

■ AUTHOR INFORMATION

Corresponding Author

*E-mail: kalyan_chattopadhyay@yahoo.com. Fax: 91 33 24146007.

Notes

The authors declare no competing financial interest.

■ ACKNOWLEDGMENTS

D.S. wishes to thank the University Grants Commission (UGC), the Government of India, for providing him a research fellowship under "UGC-research fellowship in science for meritorious students" scheme during the execution of the work. The authors also thank the UGC, the Govt. of India, for the University with potential for excellence (UPEII) scheme.

■ REFERENCES

(1) Fujishma, A.; Honda, K. *Nature* **1972**, *238*, 37−38.
(2) Liang, Y.-C.; Wang, C.-C.; Kei, C.-C.; Hsueh, Y.-C.; Cho, W.-H.; Perng, T.-P. *J. Phys. Chem. C* **2011**, *115*, 9498−9502.
(3) Chen, L.; Chen, F.; Shi, Y.; Zhang, J. *J. Phys. Chem. C* **2012**, *116*, 8579−8586.
(4) Zhou, W.; Liu, H.; Wang, J.; Liu, D.; Du, G.; Cui, J. *ACS Appl. Mater. Interfaces* **2010**, *2*, 2385−2392.
(5) Chen, X.; Liu, L.; Yu, P. Y.; Mao, S. S. *Science* **2011**, *331*, 746−750.
(6) Wang, S.; Yi, L.; Halpert, J. E.; Lai, X.; Liu, Y.; Cao, H.; Yu, R.; Wang, D.; Li, Y. *Small* **2012**, *8*, 265−271.
(7) Zhao, W.; Feng, L.; Yang, R.; Zheng, J.; Li, X. *Appl. Catal., B: Environ.* **2011**, *103*, 181−189.
(8) Lin, Y.; Jiang, Z.; Hu, X.; Zhang, X.; Fan, J. *Appl. Phys. Lett.* **2012**, *100*, 102105.
(9) Zhang, M.; Shao, C.; Mu, J.; Zhang, Z.; Guo, Z.; Zhang, P.; Liu, Y. *CrystEngComm* **2012**, *14*, 605−612.
(10) Lin, J.; Shen, J.; Wang, R.; Cui, J.; Zhou, W.; Hu, P.; Liu, D.; Liu, H.; Wang, J.; Boughton, R. I.; Yue, Y. *J. Mater. Chem.* **2011**, *21*, 5106−5113.
(11) Lu, J.; Han, Q.; Wang, Z. *Mater. Res. Bull.* **2012**, *47*, 1621−1624.
(12) He, X.; Cai, Y.; Zhang, H.; Liang, C. *J. Mater. Chem.* **2011**, *21*, 475−480.
(13) Mamun, Md. A.-A.; Kusumoto, Y.; Zannat, T.; Islam, Md. S. *Phys. Chem. Chem. Phys.* **2011**, *13*, 21026−21034.
(14) Jang, J. S.; Choi, S. H.; Kim, H. G.; Lee, J. S. *J. Phys. Chem. C* **2008**, *112*, 17200−17205.
(15) Li, X. Z.; Li, F. B.; Yang, C. L.; Ge, W. K. *J. Photochem. Photobiol., A: Chem.* **2001**, *141*, 209−217.
(16) Woan, K.; Pyrgiotakis, G.; Sigmund, W. *Adv. Mater.* **2009**, *21*, 2233−2239.
(17) Huang, H.; Li, D.; Lin, Q.; Zhang, W.; Shao, Y.; Chen, Y.; Sun, M.; Fu, X. *Environ. Sci. Technol.* **2009**, *43*, 4164−4168.
(18) Liu, S.; Wu, J.; Liu, X.; Jiang, R. *J. Mol. Catal. A: Chem.* **2010**, *332*, 84−92.
(19) Zhou, W.; Liu, H.; Wang, J.; Liu, D.; Du, G.; Han, S.; Linb, J.; Wang, R. *Phys. Chem. Chem. Phys.* **2010**, *12*, 15119−15123.
(20) Lyu, L.-M.; Huang, M. H. *J. Phys. Chem. C* **2011**, *115*, 17768−17773.
(21) Zhu, L.; Zhang, W.-D.; Chen, C.-H.; Xu, B.; Hou, M.-F. *J. Nanosci. Nanotechnol.* **2011**, *11*, 4948−4956.
(22) Xing, Z.; Geng, B.; Li, X.; Jiang, H.; Feng, C.; Ge, T. *CrystEngComm* **2011**, *13*, 2137−2142.
(23) Tang, Y.; Wee, P.; Lai, Y.; Wang, X.; Gong, D.; Kanhere, P. D.; Lim, T. T.; Dong, Z.; Chen, Z. *J. Phys. Chem. C* **2012**, *116*, 2772−2780.
(24) Zhou, W.; Liu, X.; Cui, J.; Liu, D.; Li, J.; Jiang, H.; Wang, J.; Liu, H. *CrystEngComm* **2011**, *13*, 4557−4563.
(25) Sarkar, D.; Ghosh, C. K.; Chattopadhyay, K. K. *CrystEngComm* **2012**, *14*, 2683−2690.
(26) Murray, B. J.; Li, Q.; Newberg, J. T.; Menke, E. J.; Hemminger, J. C.; Penner, R. M. *Nano Lett.* **2005**, *5*, 2319−2324.
(27) Hammond, J. S.; Gaarenstroom, S. W.; Winograd, N. *Anal. Chem.* **1975**, *47*, 2193−2199.
(28) Jeong, N. C.; Prasittichi, C.; Hupp, J. T. *Langmuir* **2011**, *27*, 14609−14614.
(29) Weaver, J. F.; Hoflund, G. B. *Chem. Mater.* **1994**, *6*, 1693−1699.
(30) Kim, J.-N.; Shin, K.-S.; Park, B.-O.; Lee, J.-H.; Kim, N.-K.; Cho, S.-H. *Smart Mater. Struct.* **2003**, *12*, 565−570.
(31) Lu, W.; Gao, S.; Wang, J. *J. Phys. Chem. C* **2008**, *112*, 16792−16800.
(32) Liu, Y.; Zhong, L.; Peng, Z.; Cai, Y.; Song, Y.; Chen, W. *CrystEngComm* **2011**, *13*, 5467−5473.
(33) Zeng, H.; Cai, W.; Liu, P.; Xu, X.; Zhou, H.; Klingshirn, C.; Kalt, H. *ACS Nano* **2008**, *2*, 1661−1670.
(34) Wang, H.; Li, G.; Jia, L.; Wang, G.; Tang, C. *J. Phys. Chem. C* **2008**, *112*, 11738−11743.
(35) Liu, B.; Huang, Y.; Wen, Y.; Du, L.; Zeng, W.; Shi, Y.; Zhang, F.; Zhu, G.; Xu, X.; Wang, Y. *J. Mater. Chem.* **2012**, *22*, 7484−7491.
(36) Xu, F.; Shen, Y.; Sun, L.; Zeng, H.; Lu, Y. *Nanoscale* **2011**, *3*, 5020−5025.
(37) Zheng, L.; Zheng, Y.; Chen, C.; Zhan, Y.; Lin, X.; Zheng, Q.; Wei, K.; Zhu, J. *Inorg. Chem.* **2009**, *48*, 1819−1825.
(38) Liang, S.; Zhu, S.; Zhu, J.; Chen, Y.; Zhang, Y.; Wu, L. *Phys. Chem. Chem. Phys.* **2012**, *14*, 1212−1222.
(39) Xiao, F.; Wang, F.; Fu, X.; Zheng, Y. *J. Mater. Chem.* **2012**, *22*, 2868−2877.
(40) Peining, Z.; Nair, A. S.; Shengjie, P.; Shengyuan, Y.; Ramakrishna, S. *ACS Appl. Mater. Interfaces* **2012**, *4*, 581−585.
(41) Li, L.; Liu, C. *CrystEngComm* **2010**, *12*, 2073−2078.
(42) Sarkar, D.; Maiti, U. N.; Ghosh, C. K.; Chattopadhyay, K. K. *Adv. Sci. Lett.* **2012**, *6*, 127−133.
(43) Fielding, L. A.; Mykhaylyk, O. O.; Armes, S. P.; Fowler, P. W.; Mittal, V.; Fitzpatrick, S. *Langmuir* **2012**, *28*, 2536−2544.
(44) Ryu, S. Y.; Noh, J. H.; Hwang, B. H.; Kim, C. S.; Jo, S. J.; Kim, J. T.; Hwang, H. S.; Baik, H. K.; Jeong, H. S.; Lee, C. H.; Song, S. Y.; Choi, S. H.; Park, S. Y. *Appl. Phys. Lett.* **2008**, *92*, 023306.
(45) Choi, H. W.; Kim, S. Y.; Kim, K.-B.; Tak, Y.-H.; Lee, J.-L. *Appl. Phys. Lett.* **2005**, *86*, 012104.
(46) Wang, X.; Koleilat, G. I.; Tang, J.; Liu, H.; Kramer, I. J.; Debnath, R.; Brzozowski, L.; Barkhouse, D. A. R.; Levina, L.; Hoogland, S.; Sargent, E. H. *Nat. Photonics* **2011**, *5*, 480−484.
(47) Liu, G.; Li, F.; Wang, D.-W.; Tang, D.-M.; Liu, C.; Ma, X.; Lu, G. Q.; Cheng, H.-M. *Nanotechnology* **2008**, *19*, 025606.
(48) Xu, H.; Xu, Y.; Li, H.; Xia, J.; Xiong, J.; Yin, S.; Huang, C.; Wan, H. *Dalton Trans.* **2012**, *41*, 3387−3394.